




Sustainable and photoresponse triboelectric nanogenerators based on 2D-gC₃N₄ and agricultural wastes

Noushin Raeisi Kheirabadi^{1,2,*} , Fathallah Karimzadeh^{1,*}, Mohammad Hossein Enayati¹, and Ehsan Naderi Kalali³

¹Department of Materials Engineering, Isfahan University of Technology, Isfahan 84156–83111, Iran

²Unconventional Computing Laboratory, University of the West of England, Bristol BS16 1QY, UK

³Faculty of Geosciences and Environmental Engineering, Southwest Jiaotong University, Chengdu 610031, China

Received: 16 May 2023

Accepted: 4 July 2023

© The Author(s) 2023

ABSTRACT

Two bio-friendly and photoactive triboelectric nanogenerators (TENG) are introduced, employing sustainable and biocompatible materials as functional components. The TENGs utilize corn husk and coconut coir fibers as the positive layers and incorporate two-dimensional graphitic carbon nitride (g-C₃N₄) nanosheets as negative layers. Upon simple biomechanical forces, the optimized devices fabricated from corn husk and coconut fibers produce a maximum output voltage of 630 V and 581 V, respectively. Under short-circuit conditions, the measured current was approximately 0.79 mA for corn husk-TENG and 11.47 mA for coconut fibers-TENG. Also, the maximum output power of 131 mW and 1980 mW were achieved over a 2 × 2 cm² area of corn husk-TENG and coconut fibers-TENG. The TENGs were also tested under blue commercial lights and UV light, and an increase of approximately 1.5 times was observed in the output voltages of both TENGs under UV light. These g-C₃N₄-based TENGs perform superior under UV illumination and can be used as nanogenerators and active photosensors. This paper proposes two eco-environmentally friendly and robust electronic devices for energy harvesting and photo-sensing applications based on two agricultural wastes, corn husk, and coconut coir fibers.

1 Introduction

Since the escalating need for energy and the depletion of fossil resources have been at odds in recent years, more emphasis has been placed on developing new energy sources. Triboelectric nanogenerators

(TENGs) with low costs, high durability, and high processability are emerging as the next generation of energy sources [1]. Triboelectric nanogenerators (TENGs) are highly adaptable electronic devices with numerous potential uses in environmental energy harvesting and self-powered electronics [2]. Concerns

Address correspondence to E-mail: Noushin.Raeisikheirabadi@uwe.ac.uk; karimzadeh_f@iut.ac.ir

over the environmental impacts of conventional electronic devices have been raised due to the rapid development of TENGs. Considering these facts, exploring alternatives to synthetic and toxic materials in electronics is crucial [2].

Many TENGs are based on synthetic polymers with stable chemical bonding, such as polytetrafluoroethylene (PTFE) [3], polydimethylsiloxane (PDMS) [4, 5], polyvinylidene fluoride (PVDF) [6], and polyethylene terephthalate (PET) [7], leading to environmental degradation and toxic chemical releases over decades. Natural materials have a wide range of applications as triboelectric materials [8]. Raw materials are easily degraded by microorganisms after they have been discarded in natural environments since they are derived or extracted from biological organisms and have excellent biocompatibility [9]. Recent research on TENGs made of raw materials concluded that their complex surface architecture significantly impacts produced charge, current, or voltage [10–12].

Agricultural by-products such as straw, rice husks, bark, bagasse and marine products such as shellfish and seaweed are sources of biological materials [13]. Among the Agricultural by-products, corn husk is one of the promising, containing a large proportion of cellulose (38.2%) and hemicellulose (44.5%), as well as a small amount of lignin (6.6%) and ash (2.8%) [14]. Corn husk, an abundant lignocellulosic waste material, possesses good flexibility, strength, moderate durability, and high elongation [15, 16]. The corn husk is traditionally burned or discarded, resulting in pollution and the waste of a cellulosic resource [17]. Coconut coir fiber consists primarily of cellulose, hemicellulose, and lignin. These fibers contain a high amount of lignin [18]. Several advantages make coconut fiber very suitable as a filler for composites, including strength, lightweight, heat resistance, salt-water resistance, low cost, and ease of accessibility [19]. Natural fibers are hydrophilic.

Furthermore, their surface contains dirt and other substances, which may affect their bonding strength. Different studies have achieved a good bond between natural fibers and the matrix [20]. One of the most common chemical treatments for natural fiber is alkali treatment. As a result of alkali treatment, most hemicellulose, lignin, waxes, and oils are expected to be removed, and the fiber surface becomes rough due to reduced fiber aggregation [21–24].

Two-dimensional materials (2D) have recently been considered for use in triboelectric nanogenerators [25]. Different 2D materials such as graphene [26], transition metal dichalcogenides (TMDs) [27], Mxene [28, 29], and some 2D hybrids, such as graphene decorated carbonized cellulose fabric [30] have been reported in fabricating TENGs, till now. Aside from the increased output, the material's thermal stability is a significant concern regarding the practical application of nanogenerators. Graphitic carbon nitride ($g\text{-C}_3\text{N}_4$) can serve as an excellent triboelectric material due to its exceptional chemical and thermal stability [31]. $g\text{-C}_3\text{N}_4$, as the first metal-free polymeric material and as the p-conjugated semiconductor, is a 2D layered material with sp^2 -hybridized carbon–nitrogen bonding [32, 33]. There are numerous reports on the photochemical and photophysical properties of $g\text{-C}_3\text{N}_4$ and its composites [34, 35], and their optoelectronic applications in the literature [36, 37]. But its applications in TENGs are rarely reported [25, 38, 39].

Here we report two novel triboelectric nanogenerators based on $g\text{-C}_3\text{N}_4$ nanosheets, corn husk, and coconut coir fibers for the first time. Nanosheets based on $g\text{-C}_3\text{N}_4$ show excellent photo-absorption properties, are biocompatible. These characteristics make them promising materials for triboelectric nanogenerators. In addition, corn husk and coconut coir fibers as by-products, agricultural wastes, and burning them cause environmental pollution. These two by-products can indeed be utilized in triboelectric nanogenerators due to their very rough surface.

2 Results and discussion

2.1 Characterization

Several hypothetical phases of carbon nitrides have been proposed, including α , β , cubic, pseudo-cubic, and graphitic, as shown in Fig. 1 [40]. As a result of the sp^2 hybridization of carbon and nitrogen, graphitic carbon nitride has the smallest direct band gap and is considered the most stable phase at ambient temperatures [41].

An XRD pattern is generally helpful for studying crystallite samples' structural phases. Figure 2c depicts the XRD pattern of the as-synthesized $g\text{-C}_3\text{N}_4$ nanosheets. The XRD equipment used in our study did exhibit some level of noise. Notwithstanding the

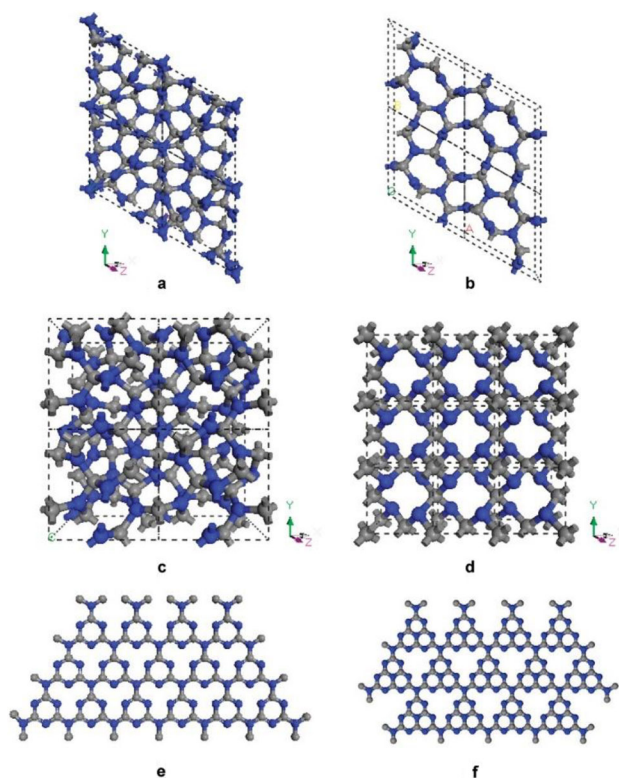


Fig. 1 The Scheme of Crystal Structure Models Proposed for Carbon Nitride **a** α - C_3N_4 ; **b** β - C_3N_4 ; **c** Cubic C_3N_4 ; **d** Pseudocubic C_3N_4 ; **e** a Graphitic- C_3N_4 Sheet Based on Melamine Building Blocks; and **f** a Graphitic- C_3N_4 Sheet Based on Melem Building Blocks. Reprinted with permission from [40]. Copyright {2009} American Chemical Society

presence of noise, The g - C_3N_4 exhibits two prominent diffraction peaks around 12.6° and 27.7° , which correspond to planes (100) and (002) (JCPDS File Number 87e1526). The first peak belongs to the tri-s-triazine unit's in-plane structures and is usually weaker than the second peak. The most substantial XRD peak is caused by the conjugated aromatic system stacking, as seen in graphite. The second peak has a higher intensity and is caused by the stacking of the conjugated aromatic system, as in graphite. There is reasonable agreement between as-synthesized CN peaks and the reported results [32, 42, 43].

The Fourier transform infrared spectroscopy (FTIR) can identify the chemical structures of organic compounds, especially those containing specific functional groups. FTIR spectra of the as-synthesized g - C_3N_4 nanosheets are shown in Fig. 2d. Broad bands of N-H stretching vibrations in the recorded spectrum at 3650 – 3000 cm^{-1} overlap with broad bands of OH stretching of the adsorbed water at this

wavelength. The absorption peaks in the range of 1639 – 1247 cm^{-1} indicate the presence of C–N and C=N stretching vibrations. Peaks in 888.98 cm^{-1} corresponded to the characteristics of *s*-triazine ring vibrations [33, 44–46]. Other absorption peaks may be caused by unreacted urea, adsorbed organic species, etc. [32, 40, 47].

SEM (Scanning electron microscopy) technique was used to evaluate the surface morphology and microstructure information of the g - C_3N_4 nanosheets and the spin-coated g - C_3N_4 and ethanol suspension on polyethylene as the negative triboelectric layer of fabricated nanogenerator. According to Fig. 3a, b, g - C_3N_4 nanosheets are homogeneously formed, and its typical laminated structure is obtained [48, 49]. After spin coating the g - C_3N_4 and ethanol suspension on polyethylene (Fig. 3c, d), due to accumulating of nanosheets on an adhesive surface, lots of pores and cavities were created, which are appropriate to trap electrons and use in a triboelectric nanogenerator device [50, 51]. EDX spectrum of the sample is shown in Fig. 3e. Based on the EDX results, the as synthesized g - C_3N_4 includes 33.79% C, 65.25% N, 0.96% O. Typical X-ray mapping images for the g - C_3N_4 are also shown in Fig. 3f.

The estimation of the absorption edge wavelengths (λ_{AE}) was conducted by extrapolating the curves towards the X-axis. These values were then used to calculate the bandgap energies of the samples using the formula E_g (eV) = $1240/\lambda_{AE}$ (nm). In our study, the absorption edge wavelengths were found to be 400 nm, resulting in a calculated bandgap energy of g - C_3N_4 of approximately 3.1 eV [32].

The SEM images (Fig. 4a–d) demonstrate that it has a rough surface and is full of bumps and depressions with protruding sharp branches similar to the tread of an elephant. So, the corn husk serves as a great layer or substrate for a triboelectric nanogenerator.

The SEM images of PVA/coconut coir fiber biocomposite with different fiber weight percent are depicted in Fig. 4e–t. Figure 4e–h represents biocomposite with 5 wt.% coconut fibers, (i–l) with 10 wt.% coconut fibers, (m–p) with 15 wt.% coconut fibers, and q–t depict biocomposite with 20 wt.% coconut fibers. As it is clear from the pictures, with the increase in the weight percentage of the coconut fibers in the composite, more volumes of fibers are placed on the surface of the composite. So, the contact surface enriches, so the friction of the two triboelectric layers augments. The number of depressions and

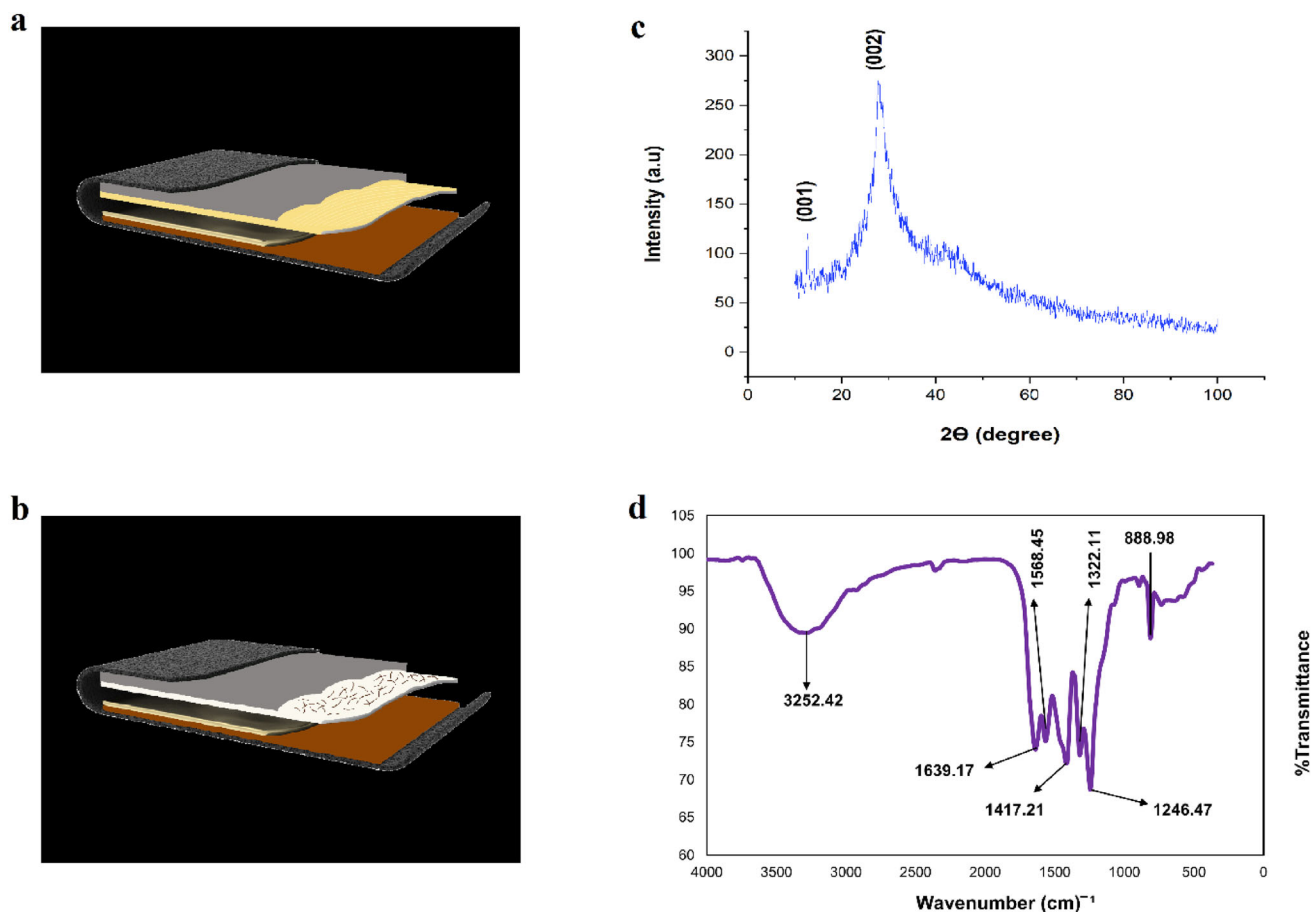


Fig. 2 **a** Schematic design of corn husk-based TENG. **b** Schematic design of coconut coir fibers based TENG. **c** XRD pattern of the as-synthesized $g\text{-C}_3\text{N}_4$ nano sheets revealing graphitic structure. **d** FTIR spectrum of the as-synthesized $g\text{-C}_3\text{N}_4$ nanosheets

protrusions increases, which provides more places to trap electric charge. According to Fig. 4m–p, this composite has a good balance between porosity and fiber percentage, making it an appropriate positive friction layer for a triboelectric nanogenerator.

2.2 Performance and application

This paper introduces two eco-friendly biocompatible triboelectric nanogenerators with vertical contact-separation mode performance. One of them is fabricated by corn husk as a positive friction layer, and another one is manufactured by polyvinyl alcohol/coconut coir fiber biocomposite as a positive friction layer as well. In both TENGs, two-dimensional $g\text{-C}_3\text{N}_4$ nanosheets were employed as a negative friction layer.

2.2.1 Corn husk TENG

Corn husk contains a large proportion of cellulose [15]. As it contains a high cellulose concentration, we employed it for a positive friction layer in the TENG Fig. 2a. In the first step, by choosing corn husk as a positive layer and Al tape as its electrode, the potential application of $g\text{-C}_3\text{N}_4$ nanosheets in triboelectric nanogenerators has been demonstrated compared with kapton as a negative triboelectric friction layer. The results of comparing the output voltage of nanogenerators made by 5 mg/ml $g\text{-C}_3\text{N}_4$ suspension and kapton both against corn husk are shown in Fig. 5a. Polyethylene tape was used as a substrate in the opposing layer in both fabricated TENGs as an intermediate layer to extend charge decay time [50, 52]. According to Fig. 5a, combining $g\text{-C}_3\text{N}_4$ nanosheets and polyethylene as a negative layer had approximately 1.5 times greater output open-circuit voltage than kapton-polyethylene.

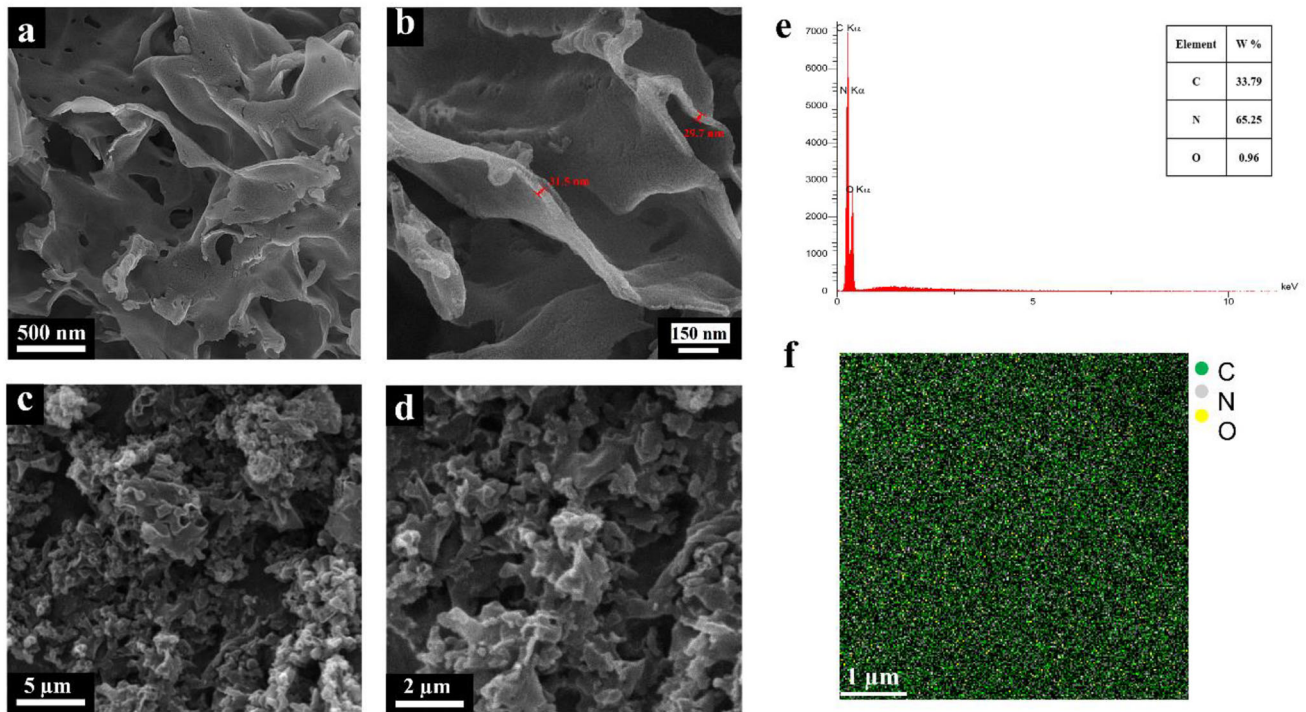


Fig. 3 SEM images of **a** and **b** as-synthesized $g\text{-C}_3\text{N}_4$ nano sheets powder in different magnifications, **c** and **d** the spin-coated of $g\text{-C}_3\text{N}_4$ and ethanol suspension on polyethylene in different

magnifications. **e** EDX spectrum of the $g\text{-C}_3\text{N}_4$. **f** X-ray mapping images for the $g\text{-C}_3\text{N}_4$

One of the influential factors in the triboelectric nanogenerator output rate is the electrode type. As the conductivity and charge trapping sites at the electrode increase, the charge density in the circuit increases, resulting in an increased nanogenerator output voltage [53]. To determine the most suitable electrode for the negative layer of the device, copper and aluminum foils, with a thickness of 100 μm , adhered to the back of the negative friction layer, and the concentration of $g\text{-C}_3\text{N}_4$ nanosheet suspension was adjusted to 1 mg/ml. Voltage diagrams of fabricated TENGs with these two electrodes are shown in Fig. 5b. By comparing their output open-circuit voltages, it can be concluded that Cu ($V_{OC} = 350$ V) performed better than Al ($V_{OC} = 300$ V) as an electrode. The reason could be due to the lower place of Cu in the triboelectric series, which means Cu has more negative triboelectric charges than Al [54]. So, for the subsequent experiments, a spin-coated suspension of $g\text{-C}_3\text{N}_4$ nanosheets on polyethylene substrate and Cu electrode was used as a negative friction layer.

Figure 5c shows that di-ionized water and ethanol were compared as the carrier phase of $g\text{-C}_3\text{N}_4$

nanosheet suspension with a 5 mg/ml concentration. The output open circuit voltages of TENGs fabricated by water and ethanol were obtained at about 600 V and 400 V, respectively. Due to the increase of 1.5 times the voltage by the water carrier, water was used as the suspension carrier liquid in the subsequent experiments.

As the concentration of $g\text{-C}_3\text{N}_4$ nanosheet suspension in di-ionized water increases, the output voltage of the nanogenerator also increases. With ascending the suspension concentration from 1 to 5 mg/ml, the average open-circuit voltage increased from 350 to 600 V (Fig. 5d). With a further increase in the suspension concentration, the output voltage did not change significantly, indicating that the surface of the PE was covered entirely with $g\text{-C}_3\text{N}_4$ nanosheet suspension. Hence, a 5 mg/ml concentration of as-synthesized suspension was used for further studies [55].

The system's performance has been evaluated based on the output voltage and corresponding output power recorded from the corn husk TENG device against different load resistances (R varying from 100 $\text{k}\Omega$ to 1 $\text{G}\Omega$) [56]. Figure 5e illustrates TENG's

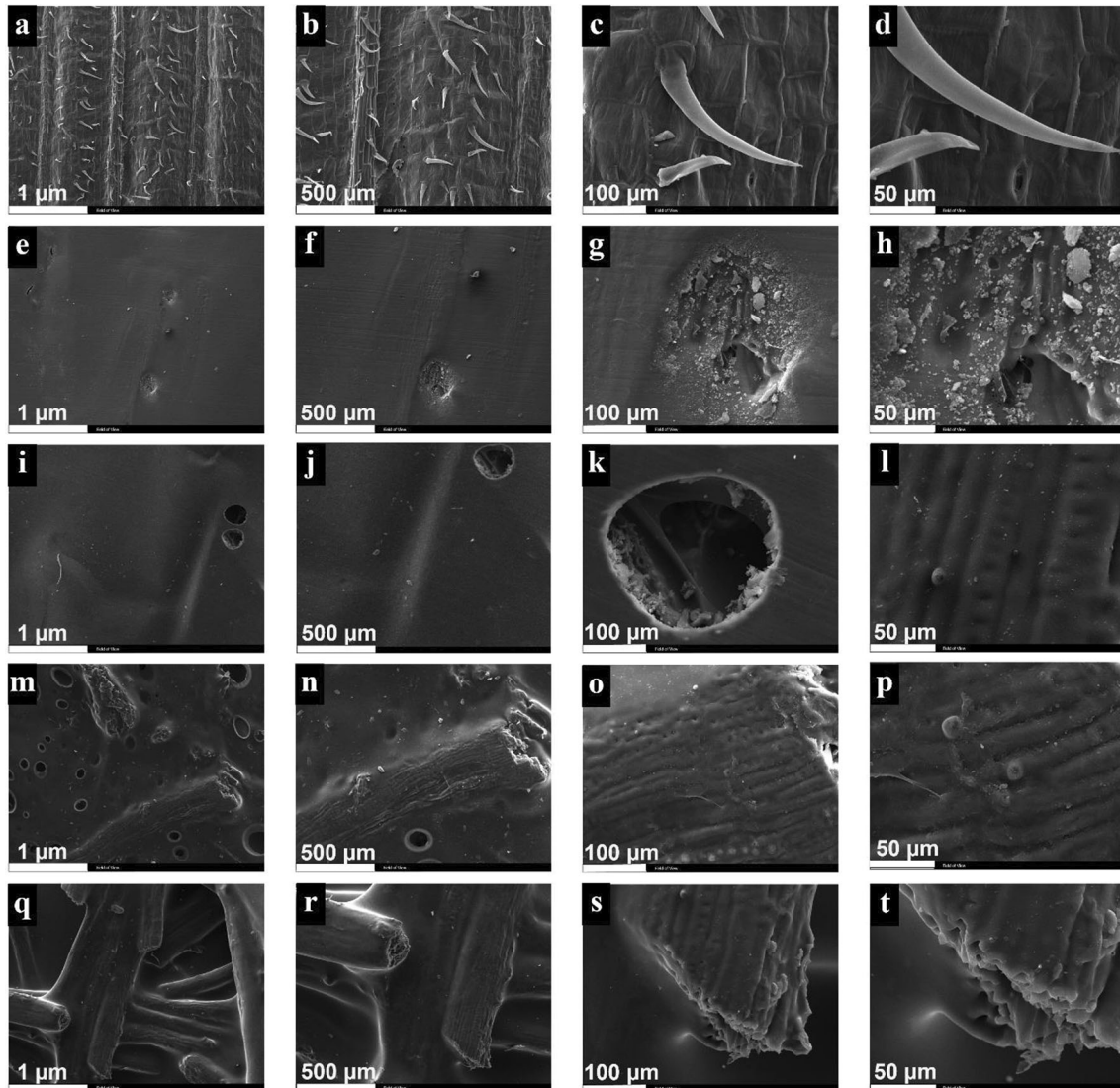


Fig. 4 SEM images of a–d corn husk, e–h coconut fiber @ PVA composite (5 wt.%), i–l coconut fiber @ PVA composite (10 wt.%), m–p coconut fiber @ PVA composite (15 wt.%), q–t) coconut fiber @ PVA composite (20 wt.%), in different magnifications

voltage and current while connected to different resistors. After increasing the resistance from 100 K Ω to 1 G Ω , the voltage gradually grew from about 80 V to 630 V. Simultaneously, the current dropped from 0.79 mA to 0.003 mA. Eventually, it became saturated at higher resistances with the highest voltage and lowest current. As shown in Fig. 5f, the maximum power does not appear at very high or very low external load values but rather somewhere in the middle. This is because the output voltage is negligible at low loads, and the output current is low at high loads, causing TENG to enter the short circuit and open circuit states [50].

Consequently, a maximum power of 131 mW and a power density of 32.75 mW/cm² were achieved at 820 K Ω , sufficient for various low-power microelectronic devices. Under short-circuit conditions, the measured current was approximately 0.79 mA (Fig. 5h). The surface charge density of the dielectric layer was computed as 0.56 $\mu\text{C}/\text{m}^2$.

As shown in Fig. 5i, the stability and durability of the corn husk TENG were assessed by applying a continuous external alternating force at 4.5 Hz. The nanogenerator was subjected to a constant force (palm), and its voltage diagram was recorded at two minutes intervals. The durability was tested during 7200 contact and separation cycles in 1600 s. The

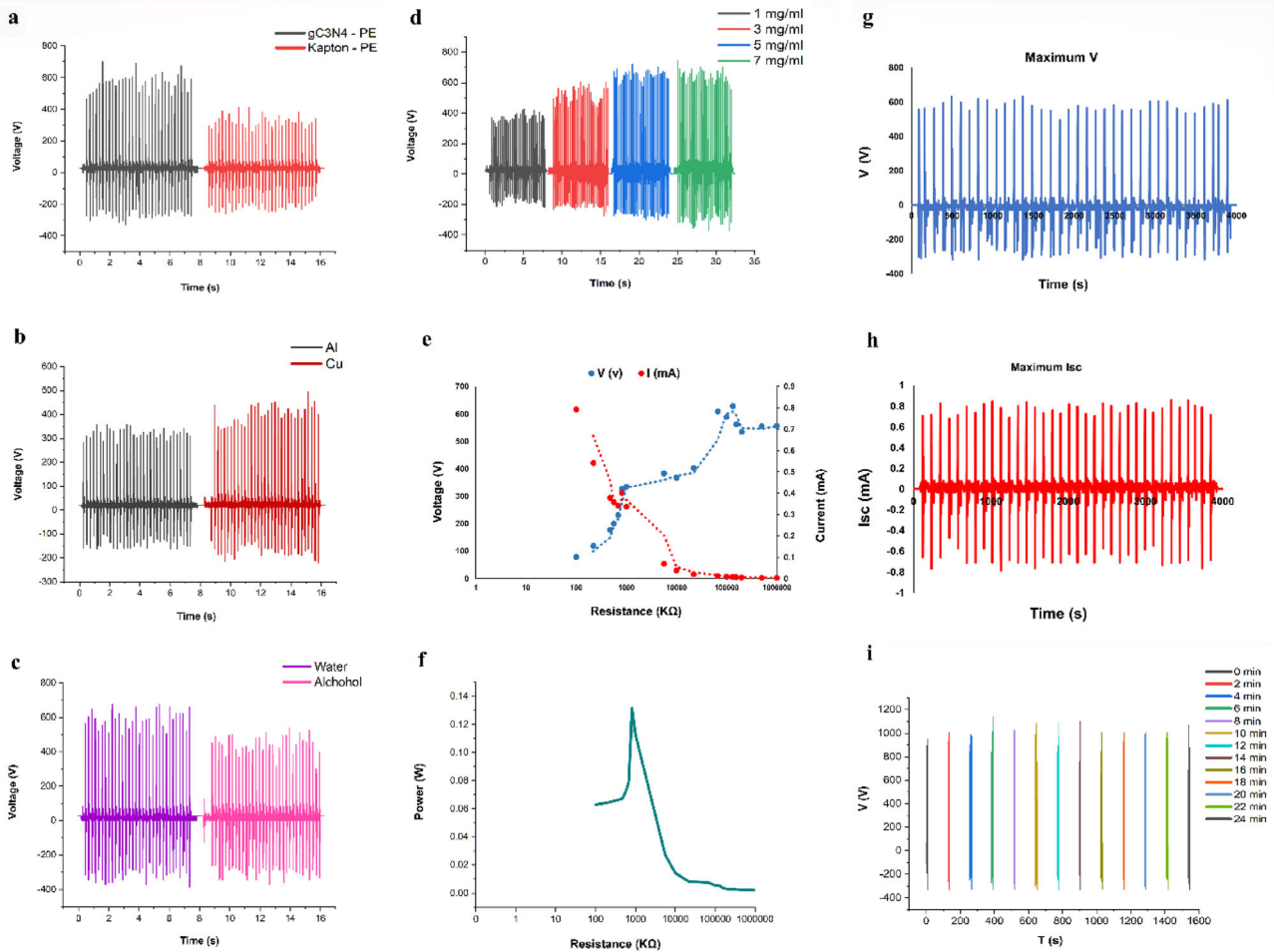


Fig. 5 Comparison of the output open-circuit voltage of corn husk nanogenerators made by **a** g-C₃N₄—PE and kapton—PE negative layers, **b** Al and Cu electrodes, **c** Water and alcohol as a suspension matrix phase to make g-C₃N₄—PE negative layer, **d** Different concentration of gC₃N₄ nanosheets suspension in the negative layer. **e** Dependence of peak *V* and *I* on external load resistance. **f** Dependence of power's peak on resistance of the

external load, indicating that maximum power output is obtained at *R* = 820 KΩ. **g** Maximum output voltage of corn husk-TENG. **h** Maximum *I*_{SC} of corn husk-TENG. **(i)** Voltage diagrams of corn husk-based nanogenerators for 7200 contact and separation cycles, showing the durability and persistence of the nanogenerator during a regular cycle

output performance of this nanogenerator was discovered to be very stable. No change in voltage signals occurred, indicating that the fabricated corn husk TENG is durable.

2.2.2 Coconut coir fiber TENG

Coconut coir fiber consists of a high amount of lignin. They are robust, lightweight, heat resistant, low cost, and have a rough and porous surface [18]. So, we utilize them in a positive friction layer. A biocompatible TENG based on polyvinyl alcohol-reinforced coconut coir fiber and 2D g-C₃N₄ nanosheets is introduced (Fig. 2b). Coconut coir fibers were

washed and, after alkaline treatment, composited one time with PVA and another by PVA and sandpaper as a substrate with 5 wt.% coir fiber. For these two fabricated positive layers, Al tape was used as electrodes, g-C₃N₄ nanosheet suspension in di-ionized water (5 mg/ml) on PE substrate, Cu electrode was chosen as negative layers, and two TENGs were fabricated. The output open-circuit results of these two TENGs are shown in Fig. 6a. As seen, the *V*_{OC} of PVA/coir fiber without any substrate is almost 1.5 times more than that of PVA/coir fiber with sandpaper substrate. So, for the following experiments, the TENG is fabricated by PVA/coir fiber without any substrate and with the Al electrode as the

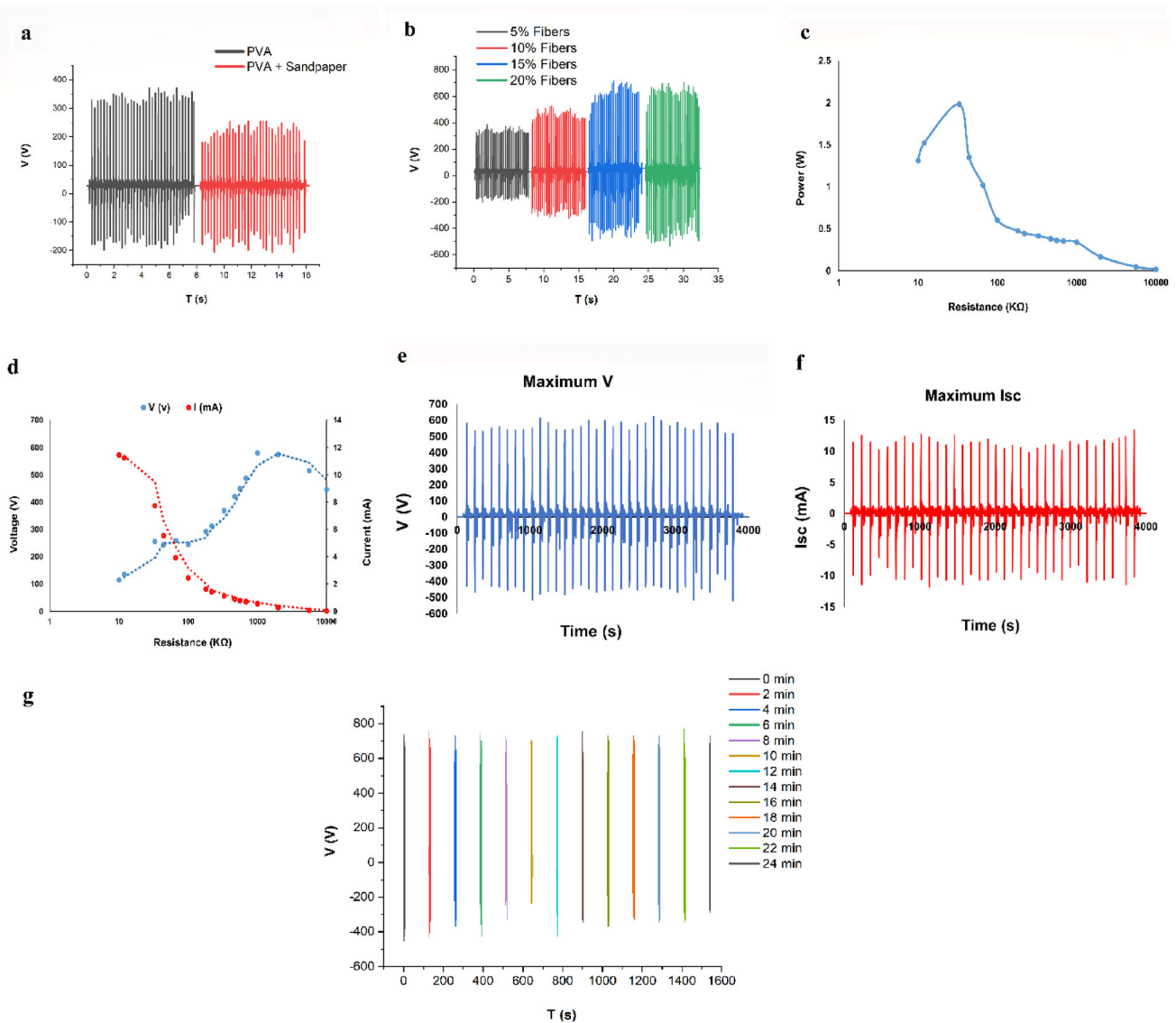


Fig. 6 Comparison of the output open-circuit voltage of coconut fibers-based nanogenerators made by **a** PVA and sandpaper-PVA as substrates of positive layers, **b** different weight percentages of coconut coir fibers in the biocomposite of a positive layer. **c** Dependence of power's peak on resistance of the external load, indicating that maximum power output is obtained at $R = 33 \text{ k}\Omega$.

positive layer and $\text{g-C}_3\text{N}_4$ nanosheets suspension in di-ionized water (5 mg/ml) on PE substrate and Cu electrode as the negative layer was chosen.

To determine the effect of the weight percentage of coconut coir fibers on the output results of the nanogenerator, four TENGs were fabricated by composites with a composition of 5, 10, 15, and 20 wt.% coconut coir fibers. According to Fig. 6b, the nanogenerator's output voltage increases with the increased weight percentage of coconut fibers. With

d Dependence of peak V and I on external load resistance. **e** Maximum output voltage of coconut fibers-TENG. **f** Maximum I_{SC} of coconut fibers-TENG. **g** Voltage diagrams of coconut fibers-based nanogenerators for 7200 contact and separation cycles, showing the durability and persistence of the nanogenerator during a regular cycle

ascending the weight percentage of coconut fibers from 5 to 15 wt.%, the average open-circuit voltage increased from about 300–600 V. With further increase in the weight percentage, the output voltage did not change significantly, indicating that the fabricated biocomposite was saturated entirely by coconut fibers [55].

Similar to the steps to optimize the resistance for the corn husk TENG, the output voltage and corresponding output power were recorded from the

coconut fibers TENG device against different load resistances (R varying from $10\text{ K}\Omega$ to $10\text{ M}\Omega$). Figure 6d, depicts TENG's voltage and current connections to other resistors. After increasing the resistance from $10\text{ K}\Omega$ to $10\text{ M}\Omega$, the average value of voltage gradually ascended from about 114.75 V to 581 V . At the same time, the current descended from 11.47 mA to 0.04 mA and eventually became saturated at higher resistances with the highest voltage and lowest current (Fig. 6e–f). Consequently, a maximum power of 1980 mW and a power density of $495\text{ mW}/\text{cm}^2$ were achieved at $33\text{ K}\Omega$. Under short-circuit conditions, the measured current was approximately 11.47 mA . The surface charge density of the dielectric layer was computed as $0.52\text{ }\mu\text{C}/\text{m}^2$.

The output results obtained from nanogenerators based on corn husk and coconut coir fibers show that although coconut fibers TENG has the same output open circuit voltage as corn husk TENG, due to its much higher short circuit current, it has much higher output power and it is appropriate for many applications in microelectronic devices. The reason for achieving varying outputs with corn husk and coconut fiber comes from the difference in the electronic structure of the two materials. In general, the triboelectric charge transfer process can be influenced by several other factors like surface states, energy level position of molecular orbitals, electron affinity, dielectric permittivity, etc. [57, 58].

The coconut coir fiber TENG's stability and durability were evaluated by applying a continuous

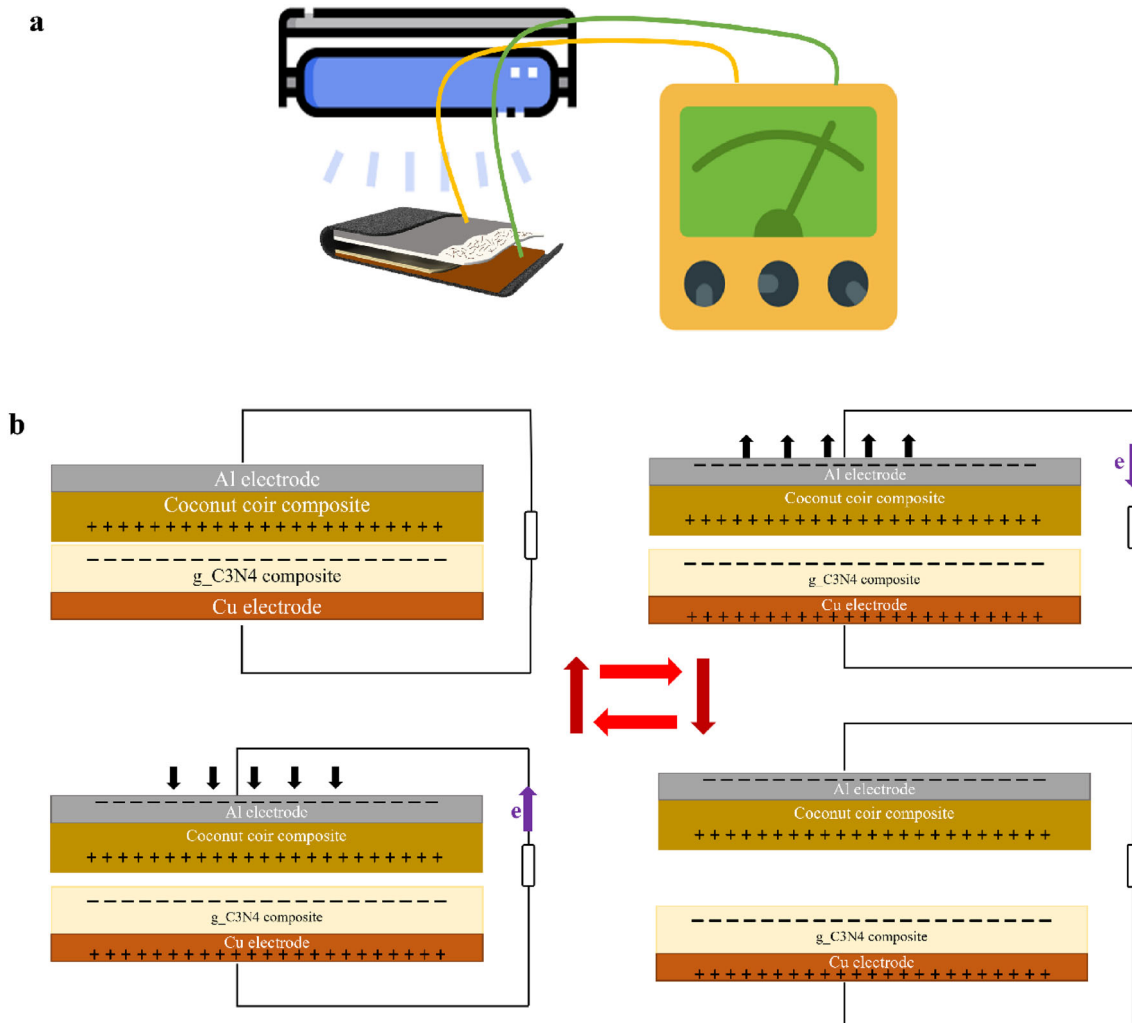


Fig. 7 a Schematic of TENG's setup, electrical contacts and circuits used for measurements under UV light. b performance model of the fabricated TENGs

external alternating force at 4.5 Hz Fig. 6g. The nanogenerator was subjected to a constant force (palm), and the voltage diagram was recorded every two minutes. The durability was tested during 7200 contact and separation cycles in 1600 s. This nanogenerator's output performance was discovered to be very stable. There was no change in voltage signals, indicating that the fabricated coir fibers TENG is long-lasting.

2.2.3 TENGs application

Schematic of TENG's setup, electrical contacts and circuits used for measurements under UV light illustrated in Fig. 7a. The performance model of the

fabricated TENGs is a vertical separation contact model, as shown in Fig. 7b.

The LED lamp test demonstrated corn husk and coconut fibers TENG's ability to generate electricity. These nanogenerators can turn on 55 blue light LEDs simultaneously, as illustrated in Figs. 8a, b. Figures 8c–f depict the maximum output voltage of the devices when they are under a UV (366 nm) light source compared to the visible light. Figure 9 represents the maximum output voltage of two fabricated TENGs under 340 nm, 366 nm, 390 nm, 420 nm, visible light sources, and in darkness. Considering that $g\text{-C}_3\text{N}_4$ has a maximum absorption below 390 nm in the UV–visible absorption spectrum, it is

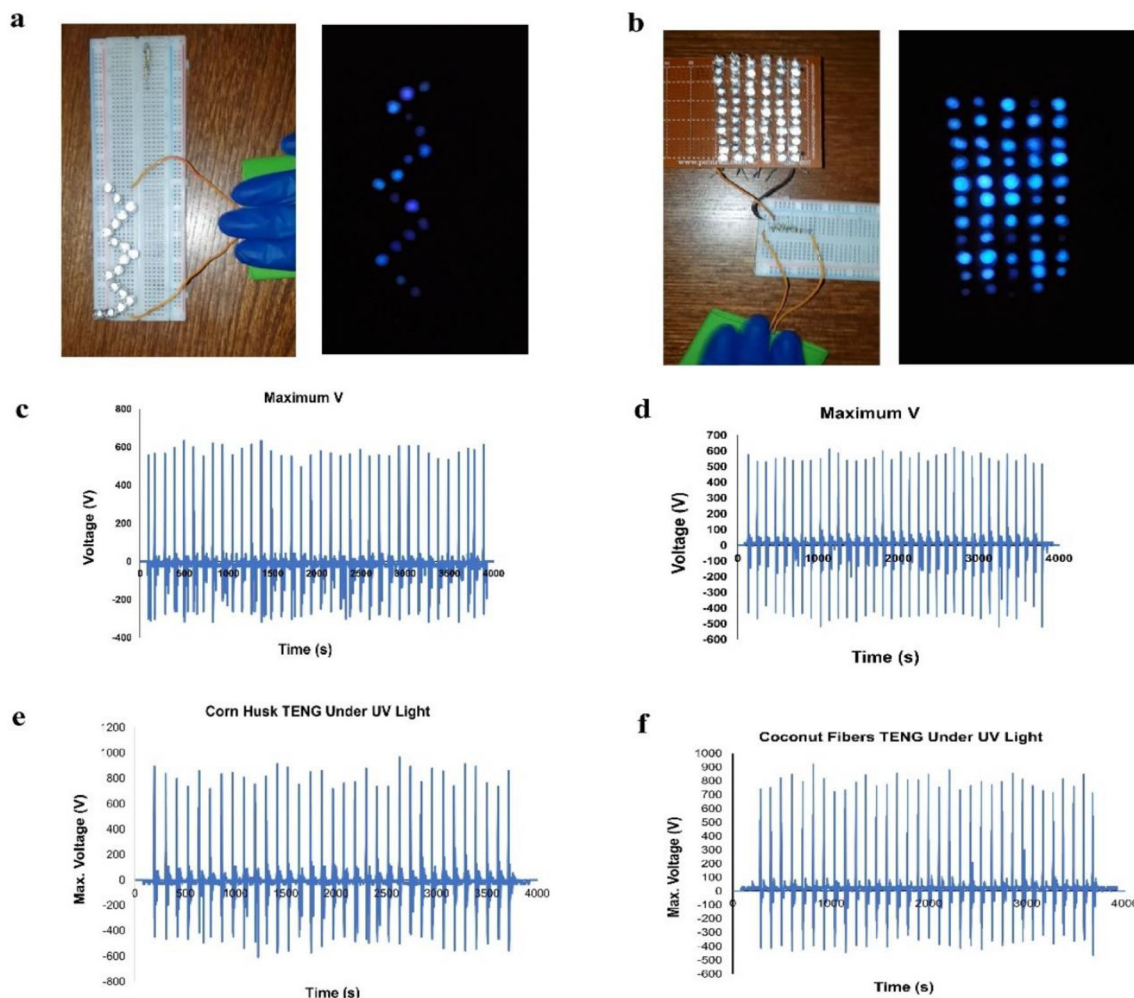
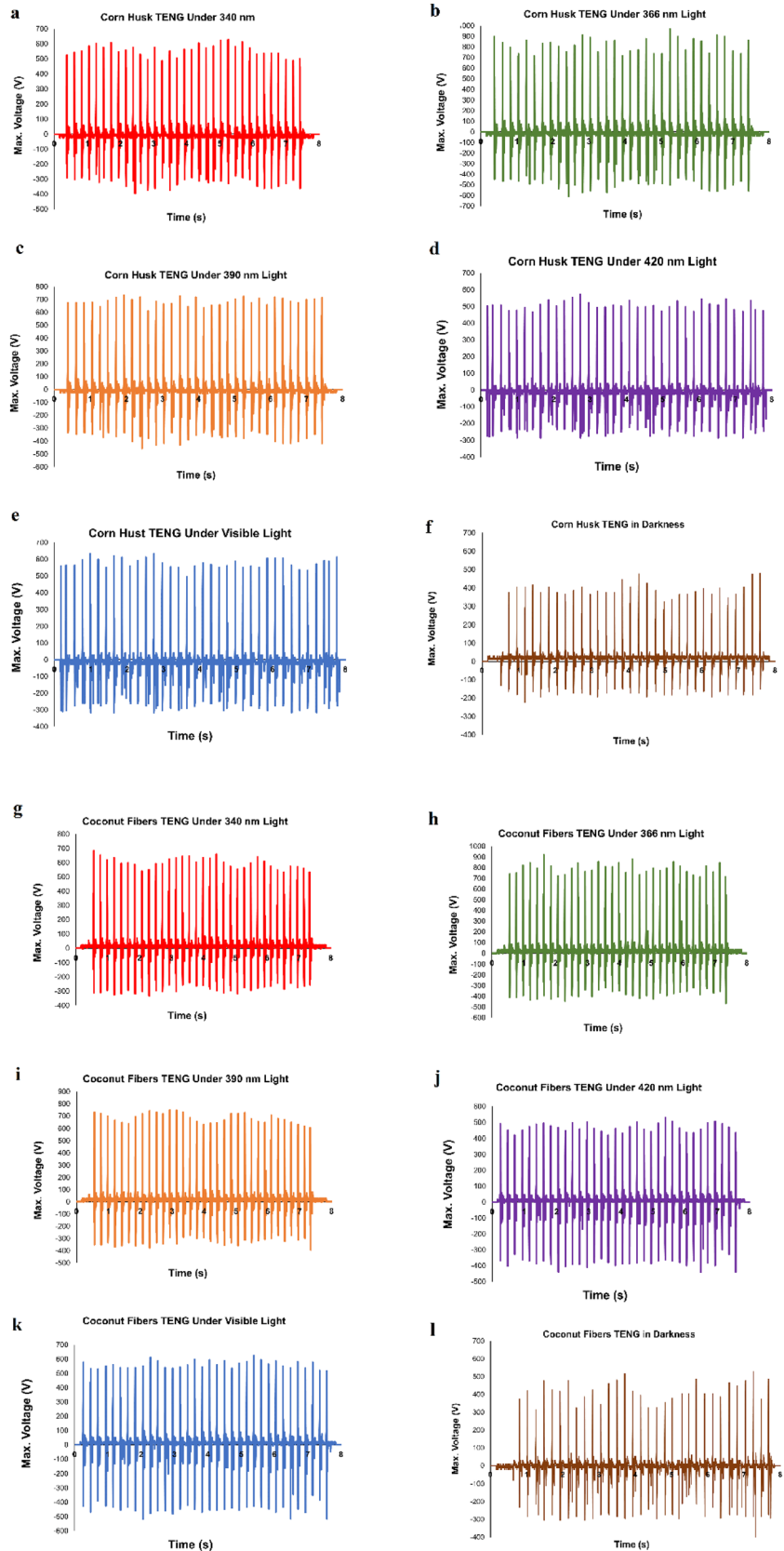


Fig. 8 **a** corn husk-TENG with $2 \times 2 \text{ cm}^2$ dimensions, connected in series to 18 commercial blue LEDs. **b** coconut fibers-TENG with $2 \times 2 \text{ cm}^2$ dimensions, connected to 55 commercial blue LEDs, illuminates the lamps using finger pressing. **c** Maximum output voltage diagram of corn husk-TENG under visible light.

d Maximum output voltage diagram of coconut fibers-TENG under visible light. **e** Maximum output voltage diagram of corn husk-TENG under UV light. **f** Maximum output voltage diagram of coconut fibers-TENG under UV light

Fig. 9 Maximum output voltage diagrams of corn husk-TENG under **a** 340 nm light, **b** 366 nm light, **c** 390 nm light, **d** 420 nm light, **e** visible light, **f** in darkness. Maximum output voltage diagrams of coconut fibers-TENG under **g** 340 nm light, **h** 366 nm light, **i** 390 nm light, **j** 420 nm light, **k** visible light, **l** in darkness



expected that the energy of a 420 nm light source will not be sufficient to excite electrons to higher energy levels. The output voltage is increased under 366 nm UV illumination to approximately 1.5 times than the visible light and 2 times than the darkness. In the presence of UV illumination, g-C₃N₄ nanosheets photo-generate excess electrons due to the excitation of valence bands into conduction bands [59, 60]. The availability of these photogenerated charges, in addition to the triboelectric charges, makes more triboelectric charges on the friction layers. While illumination occurs, UV-excited electrons are transferred to the vacant states in the positive friction layer, resulting in a higher output voltage [25].

The responsivity (R), which is an important performance metric, of the fabricated nanogenerators was determined using the following equation. Where ΔV represents the voltage difference observed between dark and light conditions, A denotes the effective area of the device, and P represents the incident light intensity [61].

$$R = \Delta V / A.P$$

When subjected to an incident illumination of 10 mW/cm², the responsivity value was found to be about 10⁴ V/W. This value is comparable with the reported responsivity of a gC₃N₄/polypropylene-based TENG device [25] and is similar to what has been reported for hybrid perovskite/pentacene-based TENG device in similar incident light intensity [61].

Since g-C₃N₄ has superior photo-absorption capability, it can be an attractive material for TENG devices. In this regard, the operation of TENGs based on g-C₃N₄ presents an exciting challenge since incident radiation modulates the surface charge density, which can also be used as a photodetector. Only a few reports describe using TENG as a power source and a photodetector simultaneously [62–64].

In addition, due to pyrolysis at a high temperature, g-C₃N₄-based TENG is extremely thermally and chemically stable, making it capable of withstanding harsh environments. Hence, TENGs based on gC₃N₄ offer excellent prospects for robust and photoactive devices for future energy applications.

While normal UV nanosensors are primarily designed to detect and measure ultraviolet (UV) light, fabricated Photoresponse Triboelectric Nanogenerators based on 2D-gC₃N₄ offer a unique combination of

energy harvesting and UV sensing capabilities. In contrast to normal UV nanosensors that solely focus on UV detection, these fabricated TENGs offer the added advantage of simultaneous energy harvesting and UV sensing. This dual functionality makes them suitable for applications in self-powered devices, wearable electronics, and portable energy sources, particularly in outdoor or well-lit environments where UV light is abundant. Overall, our research introduces eco-environmentally friendly and robust electronic devices that not only harvest energy from mechanical forces but also serve as active photosensors, highlighting their potential for energy harvesting and photo-sensing applications.

3 Conclusion

A novel, eco-friendly, photoactive triboelectric nanogenerator was designed, fabricated, and characterized based on agricultural waste and two-dimensional g-C₃N₄ nanosheets. Two triboelectric nanogenerators were investigated based on corn husk and coconut coir fibers, with contact separation mode configuration. The coconut coir fibers TENG had superior properties with a maximum power of 1980 mW and I_{SC} of 11.47 mA. The electrical output of the TENG based on coconut fibers was capable of directly powering at least 55 high-power blue LEDs. Also, g-C₃N₄'s photoactive property manifests itself in a 1.5-fold enhancement in TENG output under UV (366 nm) illumination, showing the device's dual function as a nanogenerator for microelectronic devices as well as a UV photodetector.

4 Experimental section/methods

4.1 Materials

Corn husk and coconut coir fibers were prepared from a local market. Copper plate (thickness: 100 μm), aluminum foil (thickness: 70 μm), meshed surface aluminum tape, 3 M polyethylene tape (PE tape), and ethylene vinyl acetate (EVA) foam as an arc-shaped supporting structure were prepared from a local market and used without any further purification. Urea, sodium hydroxide (NaOH), and polyvinyl alcohol (PVA) ($M = 20,000$) were prepared from Merck.

4.2 g-C₃N₄ synthesis

To synthesize g-C₃N₄ nanosheets, urea was thoroughly powdered in an agate mortar, and 25 g of the powder was placed in an alumina crucible and covered. The sample begins to heat up to 550 °C at a rate of 2 °C/min in an air atmosphere. The temperature was held at this level for 3 h until the yellow g-C₃N₄ was achieved. The obtained g-C₃N₄ was powdered in an agate mortar for the next steps [32, 65].

Due to preparing four suspensions of gC₃N₄ in H₂O with different concentrations, 10, 30, 50, and 70 mg of gC₃N₄ were mixed with 10 ml di-ionized water and placed in an ultrasonic bath for 30 min. Then these four suspensions were spin-coated (2000 rpm) on four 3 M polyethylene tape (Fig. 10a).

4.3 Polyvinyl alcohol/coconut coir fibers biocomposite synthesis

4.3.1 Alkali treatment of fibers

10 g of coconut coir fibers were milled into micrometer pieces and soaked in distilled water at 70 °C for 1 h. After removing the water, the fibers were dried in an oven at 80 °C until they reached a constant weight. In 100 ml of distilled water, 5 g of NaOH pellets were dissolved, then the solution was stirred. After drying, the fibers were immersed in the NaOH solution for 6 h. The final step involved removing the fibers from the solution, washing, and drying them in the oven at 80 °C to ensure constant weight [66, 67].

4.3.2 Composites preparation

PVA granules were completely dissolved in distilled water in four different beakers at a 1:10 ratio while

stirring and heating at 180 °C to make four other PVA and coconut coir fiber composites. In the respective beakers, four different fiber compositions (5, 10, 15, and 20 weight percent) were added to the PVA solution and stirred until the fibers were evenly distributed. The solutions were then poured into the moulds and dried in an oven at 70 °C to solidify. Finally, the solids were pressed to form four different combination composite films [66].

5 TENGs fabrication

In the first stage, for fabricating the negative layer, a 2*2 cm² polyethylene tape was cut, and an aluminum/copper foil of the same size adhered to the backside of the polyethylene tape. On the front side, 1 ml of gC₃N₄ suspension in Ethanol/water was spin-coated (Fig. 10c).

Two positive triboelectric layers were prepared from corn husk and a biocomposite of polyvinyl alcohol (PVA) polymer and coconut coir fibers. Corn husk was washed and cleaned with di-ionized water and ethanol to make the first positive layer and then cut in 2*2 cm² size. A meshed surface of aluminum tape of the same size adhered to one side of the corn husk. Due to preparing the second positive layer (coconut coir fiber reinforced polyvinyl alcohol as a biodegradable composite), the meshed surface aluminum tapes with the size of 2*2 cm² were stuck to each composite film. In all stages of comparison and optimization of layers, the applied force of ~ 13 N was adjusted using fingers and palm.

5.1 Equipment and characterization

The coating was done with the spin coating backer vCOAT4-HS. A digital scientific oscilloscope

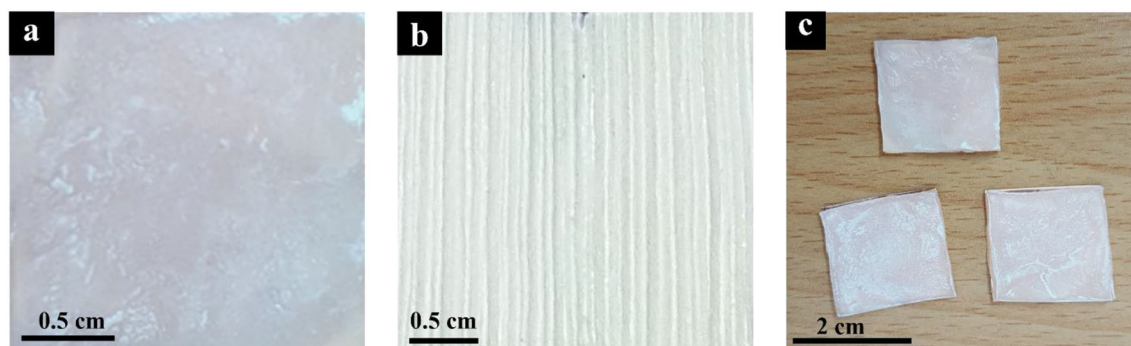


Fig. 10 Images of **a** Spin coated gC₃N₄ nanosheets on PE, **b** Corn husk, **c** Spin-coated gC₃N₄ nanosheets on PE, with the copper electrode as a negative layer

(MEGATEK-DSO5070) with a 10 M Ω probe and a Keithley 2450 Sourcemeter were used to measure output performance. The surface structure of the samples was examined by scanning electron microscopy (SEM, Philips XL30 SERIES).

To identify the synthesized gC₃N₄, Fourier-transform infrared spectroscopy (FT-IR) was performed with a Bruker Tensor 27 over a range of 400–4000 cm⁻¹ with a resolution of 2 cm⁻¹. A Philips X-beam diffractometer was used to obtain X-ray diffraction patterns of the specimens over a 2 θ range of 10–90° using CuK α radiation ($\lambda = 1.54056 \text{ \AA}$).

Acknowledgements

This research was funded by the Iran National Science Foundation (INSF), under Ph.D. program grant No. 98029358.

Author contributions

NRK: conceptualization, methodology, software, visualization, writing—original draft. FK: validation, supervision, project administration, writing—review and editing. MHE: validation, supervision, project administration, writing—review and editing. ENK: validation, writing—review and editing.

Data availability

The datasets made and analyzed during the current study are available from the corresponding author.

Declarations

Conflict of interest The authors have no relevant financial or non-financial interests to disclose.

Ethical approval This research does not involve Human Participants and/or Animals.

Open Access This article is licensed under a Creative Commons Attribution 4.0 International License, which permits use, sharing, adaptation, distribution and reproduction in any medium or format, as long as you give appropriate credit to the original author(s) and the source, provide a link to the Creative Commons licence, and indicate if

changes were made. The images or other third party material in this article are included in the article's Creative Commons licence, unless indicated otherwise in a credit line to the material. If material is not included in the article's Creative Commons licence and your intended use is not permitted by statutory regulation or exceeds the permitted use, you will need to obtain permission directly from the copyright holder. To view a copy of this licence, visit <http://creativecommons.org/licenses/by/4.0/>.

References

1. X. Li, C. Jiang, Y. Ying, J. Ping, *Adv. Energy Mater.* **10**, 2002001 (2020)
2. F.G. Torres, G.E. De-la-Torre, *Carbohydr. Polym.* **251**, 117055 (2021)
3. B. Zhang, Y. Tang, R. Dai, H. Wang, X. Sun, C. Qin, Z. Pan, E. Liang, Y. Mao, *Nano Energy* **64**, 103953 (2019)
4. Y. Liu, N. Sun, J. Liu, Z. Wen, X. Sun, S.T. Lee, B. Sun, *ACS Nano* **12**, 2893 (2018)
5. F. Salemia, F. Karimzadeha, M. A., *Nano-, undefined bio-, undefined info, and undefined 2022*. Spiedigitalibrary.Org (n.d.).
6. L. Zhang, B. Zhang, J. Chen, L. Jin, W. Deng, J. Tang, H. Zhang, H. Pan, M. Zhu, W. Yang, Z.L. Wang, *Adv. Mater.* **28**, 1650 (2016)
7. Z. Zhao, X. Pu, C. Du, L. Li, C. Jiang, W. Hu, Z.L. Wang, *ACS Nano* **10**, 1780 (2016)
8. S. Rajala, T. Siponkoski, E. Sarlin, M. Mettänen, M. Vuoriluoto, A. Pammo, J. Juuti, O.J. Rojas, S. Franssila, S. Tuukkanen, *ACS Appl. Mater. Interfaces* **8**, 15607 (2016)
9. U. de Corato, I. de Bari, E. Viola, M. Pugliese, *Renew. Sustain. Energy Rev.* **88**, 326 (2018)
10. S.H. Shin, Y.H. Kwon, Y.H. Kim, J.Y. Jung, M.H. Lee, J. Nah, *ACS Nano* **9**, 4621 (2015)
11. S. Wang, Y. Zi, Y.S. Zhou, S. Li, F. Fan, L. Lin, Z.L. Wang, *J. Mater. Chem. A* **4**, 3728 (2016)
12. Y. Yu, X. Wang, *Extreme Mech. Lett.* **9**, 514 (2016)
13. V. Slabov, S. Kopyl, M.P.S. dos Santos, A.L. Kholkin, *Nano-Micro Lett.* **12**, 1 (2020)
14. B. Barl, C.G. Biliaderis, E.D. Murray, A.W. Macgregor, *J. Sci. Food Agric.* **56**, 195 (1991)
15. N. Reddy, Y. Yang, *Green Chem.* **7**, 190 (2005)
16. <https://ojs.cnr.ncsu.edu/index.php/BioRes/article/view/9116>.
17. L. Hu, H. Du, C. Liu, Y. Zhang, G. Yu, X. Zhang, C. Si, B. Li, H. Peng, *ACS Sustain. Chem. Eng.* **7**, 1327 (2019)
18. M. Arsyad, I.N.G. Wardana et al., *Matéria* **20**, 169 (2015)

19. M.F. Rosa, B. Chiou, E.S. Medeiros, D.F. Wood, T.G. Williams, L.H.C. Mattoso, W.J. Orts, S.H. Imam, *Bioresour. Technol.* **100**, 5196 (2009)
20. D. Savita, V. Preeti, *Adv. Appl. Sci. Res.* **3**, 1463 (2012)
21. https://ojs.cnr.ncsu.edu/index.php/BioRes/article/view/BioRes_05_2_1143_Carvalho_MVC_Chem_Mod_HIPS_corn_composites/632.
22. <http://nopr.niscair.res.in/handle/123456789/14634>.
23. <http://nopr.niscair.res.in/handle/123456789/15888>.
24. <https://publisher.uthm.edu.my/ojs/index.php/ijie/article/view/191>.
25. S. Bayan, D. Bhattacharya, R.K. Mitra, S.K. Ray, *Nanoscale* **12**, 21334 (2020)
26. S. Kim, M.K. Gupta, K.Y. Lee, A. Sohn, T.Y. Kim, K. Shin, D. Kim, S.K. Kim, K.H. Lee, H. Shin, *Adv. Mater.* **26**, 3918 (2014)
27. M. Seol, S. Kim, Y. Cho, K. Byun, H. Kim, J. Kim, S.K. Kim, S. Kim, H. Shin, S. Park, *Adv. Mater.* **30**, 1801210 (2018)
28. C. Jiang, C. Wu, X. Li, Y. Yao, L. Lan, F. Zhao, Z. Ye, Y. Ying, J. Ping, *Nano Energy* **59**, 268 (2019)
29. X. Luo, L. Zhu, Y. Wang, J. Li, J. Nie, Z.L. Wang, *Adv. Funct. Mater.* **31**, 2104928 (2021)
30. R. Wu, L. Ma, A. Patil, Z. Meng, S. Liu, C. Hou, Y. Zhang, W. Yu, W. Guo, X.Y. Liu, *J. Mater. Chem. A* **8**, 12665 (2020)
31. G. Dong, Y. Zhang, Q. Pan, J. Qiu, *J. Photochem. Photobiol. C* **20**, 33 (2014)
32. N. Raeisi-Kheirabadi, A. Nezamzadeh-Ejhieh, *Int. J. Hydrogen Energy* **45**, 33381 (2020)
33. K.R. Reddy, C.H.V. Reddy, M.N. Nadagouda, N.P. Shetti, S. Jaesool, T.M. Aminabhavi, *J. Environ. Manag.* **238**, 25 (2019)
34. J. Fu, J. Yu, C. Jiang, B. Cheng, *Adv. Energy Mater.* **8**, 1701503 (2018)
35. N.F.F. Moreira, M.J. Sampaio, A.R. Ribeiro, C.G. Silva, J.L. Faria, A.M.T. Silva, *Appl. Catal. B* **248**, 184 (2019)
36. S. Bayan, N. Gogurla, A. Midya, S.K. Ray, *Carbon N Y* **108**, 335 (2016)
37. S. Bayan, N. Gogurla, A. Midya, A. Singha, S.K. Ray, *Nanotechnology* **28**, 485204 (2017)
38. S. Bayan, S. Pal, S.K. Ray, *Nano Energy* **94**, 106928 (2022)
39. S. Bayan, D. Bhattacharya, R.K. Mitra, S.K. Ray, S.K. Ray, *Nanotechnology* **31**, 365401 (2020)
40. K. Maeda, X. Wang, Y. Nishihara, D. Lu, M. Antonietti, K. Domen, *J. Phys. Chem. C* **113**, 4940 (2009)
41. B. Molina, L.E. Sansores, *Modern Phys. Lett.* **13**, 193 (2011)
42. J. Cao, C. Qin, Y. Wang, H. Zhang, G. Sun, Z. Zhang, *Materials* **10**, 604 (2017)
43. S.M.A. Moneim, T.A. Gad-Allah, M.F. El-Shahat, A.M. Ashmawy, H.S. Ibrahim, *J. Environ. Chem. Eng.* **4**, 4165 (2016)
44. S. Ghattavi, A. Nezamzadeh-Ejhieh, *Compos. B Eng.* **183**, 107712 (2020)
45. P. Chen, L. Chen, S. Ge, W. Zhang, M. Wu, P. Xing, T.B. Rotamond, H. Lin, Y. Wu, Y. He, *Int. J. Hydrogen Energy* **45**, 14354 (2020)
46. A. Mishra, A. Mehta, S. Basu, N.P. Shetti, K.R. Reddy, T.M. Aminabhavi, *Carbon N Y* **149**, 693 (2019)
47. S. Kumar, T. Surendar, A. Baruah, V. Shanker, *J. Mater. Chem. A* **1**, 5333 (2013)
48. Y. Wang, S. Zhao, Y. Zhang, J. Fang, W. Chen, S. Yuan, Y. Zhou, *ACS Sustain. Chem. Eng.* **6**, 10200 (2018)
49. J. Lu, Y. Wang, J. Huang, L. Cao, J. Li, G. Hai, Z. Bai, *Mater. Sci. Eng. B* **214**, 19 (2016)
50. M.A. Jalili, Z. Khosroshahi, N.R. Kheirabadi, F. Karimzadeh, M.H. Enayati, *Nano Energy* **90**, 106581 (2021)
51. A.D. Sedeh, F. Karimzadeh, M. Kharaziha, *Sustain. Energy Technol. Assess.* **56**, 103058 (2023)
52. N.R. Kheirabadi, F. Karimzadeh, M.H. Enayati, E.N. Kalali, *Adv. Electron. Mater.* **9**, 2200839 (2022)
53. L. Gao, X. Chen, S. Lu, H. Zhou, W. Xie, J. Chen, M. Qi, H. Yu, X. Mu, Z.L. Wang, Y. Yang, *Adv. Energy Mater.* **9**, 1902725 (2019)
54. H. Zou, Y. Zhang, L. Guo, P. Wang, X. He, G. Dai, H. Zheng, C. Chen, A.C. Wang, C. Xu, Z.L. Wang, *Nat. Commun.* **10**, 1 (2019)
55. Q. Wang, M. Chen, W. Li, Z. Li, Y. Chen, Y. Zhai, *Nano Energy* **41**, 128 (2017)
56. M.A. Jalili, F. Karimzadeh, M.H. Enayati, E.N. Kalali, N.R. Kheirabadi, *Adv. Electron. Mater.* **9**, 2201348 (2023)
57. Q. Guo, Y. Zhang, J. Qiu, G. Dong, *J. Mater. Chem. C* **4**, 6839 (2016)
58. X. Zhang, L. Chen, Y. Jiang, W. Lim, S. Soh, *Chem. Mater.* **31**, 1473 (2019)
59. S. Bayan, N. Gogurla, A. Ghorai, S.K. Ray, *ACS Appl. Nano Mater.* **2**, 3848 (2019)
60. S. Bayan, A. Midya, N. Gogurla, A. Singha, S.K. Ray, *J. Phys. Chem. C* **121**, 19383 (2017)
61. X. De Yang, J.J. Han, G. Wang, L.P. Liao, C.Y. Xu, W. Hu, P. Li, B. Wu, A.M. Elseman, G.D. Zhou, Q.L. Song, *J. Mater. Sci.* **54**, 9004 (2019)
62. L. Su, Z.X. Zhao, H.Y. Li, J. Yuan, Z.L. Wang, G.Z. Cao, G. Zhu, *ACS Nano* **9**, 11310 (2015)
63. L. Su, H.Y. Li, Y. Wang, S.Y. Kuang, Z.L. Wang, G. Zhu, *Nano Energy* **31**, 264 (2017)
64. Y. Pang, F. Xue, L. Wang, J. Chen, J. Luo, T. Jiang, C. Zhang, Z.L. Wang, Y. Pang, F. Xue, L. Wang, J. Chen, J. Luo, T. Jiang, C. Zhang, Z.L. Wang, *Adv. Sci.* **3**, 1500419 (2016)
65. X. Wang, K. Maeda, X. Chen, K. Takanebe, K. Domen, Y. Hou, X. Fu, M. Antonietti, *J. Am. Chem. Soc.* **131**, 1680 (2009)

66. I. Kong, J.T.B. Shang, K.Y. Tshai, ARPN J. Eng. Appl. Sci. **11**, 135 (2016)
67. T. Yu, J. Ren, S. Li, H. Yuan, Y. Li, Compos. A **41**, 499 (2010)

Publisher's Note Springer Nature remains neutral with regard to jurisdictional claims in published maps and institutional affiliations.